Multielectron inner-shell photoexcitation in absorption spectra of Kr: Theory and experiment

Stephen J. Schaphorst,* Alojz F. Kodre,† Johannes Ruscheinski, and Bernd Crasemann
Department of Physics, University of Oregon, Eugene, Oregon 97403

Teijo Åberg and Jukka Tulkki
Laboratory of Physics, Helsinki University of Technology, 02150 Espoo, Finland

Mau Hsiung Chen
High-Temperature Physics Division, Lawrence Livermore National Laboratory, Livermore, California 94550

Yoshiro Azuma
Physics Division, Argonne National Laboratory, Argonne, Illinois 60439

George S. Brown
Department of Physics, University of California, Santa Cruz, California 95064
(Received 22 September 1992)

The probability of Kr 1*s* photoionization alone and accompanied by 4*p*, 3*d*, 3*p*, 2*s*, and 2*s*4*p* excitations has been calculated as a function of photon energy in the vicinity of the respective thresholds; pertinent energies have been computed including relativistic, quantum-electrodynamic, and relaxation effects. Sharp features from two-electron excitations are expected in absorption spectra only if at least one of the electrons undergoes a transition to a bound state; this becomes less probable in inner shells. An absorption-spectrometry experiment on Kr has been performed with synchrotron radiation; results generally confirm the predictions but also point toward refinements that are required in the theory and the need for improvements in techniques and synchrotron-radiation sources.

PACS number(s): 32.80.Fb

I. INTRODUCTION

In atomic inner-shell photoionization, more than one electron can be excited with significant probability. Final states are thus produced that can be described approximately by configurations formed by removal of a core electron and excitation of additional electrons to higher bound states (shakeup) or to the continuum (shakeoff) [1–4]. These multiple excitation processes can be identified through the satellites they produce in photoelectron spectra [1,5–7] and in the Auger and x-ray spectra emitted when the excited states decay [2,3,8–10] as well as, in some cases, by features in absorption spectra [11].

The many-electron processes induced by photon impact epitomize the limitations of the conventional most tractable models of atomic structure. Since the photon-electron interaction is described by a one-electron operator, the frozen-core, central-field model does not predict changes of state of more than one electron. Direct multiple-excitation processes are thus a result of electron-electron correlation. Their study, especially near threshold [12], can therefore provide useful insight into electron correlation mechanisms [7,13–16].

Considerations of the role of multielectron or multivacancy processes in the origin of x-ray satellites have a venerable history. In 1921, Wentzel [17] held double-electron processes responsible for *K* x-ray satellites. Heisenberg [18] formulated selection rules for two-electron transitions in 1925, lamenting the ambiguity of a "mechanical" model of the atom—apparently he was to learn of electron spin but later in the year. Druyvesteyn [19] showed convincingly that the [satellite] "x-ray spectrum of the second kind" originates from atoms with two inner-shell vacancies. Richtmyer [20] suggested two-electron–one-photon transitions as a source of x-ray satellites. Bloch [21] followed up on this suggestion with theoretical considerations of double-electron transitions in x-ray spectra. Specifically, he used the sudden approximation to calculate the probability of outer-electron excitation accompanying 1*s* ionization, inferring that a subsequent two-electron transition might lead to emission of a satellite photon. Actually, two-electron–one-photon transitions, causing "Wölfli lines," were discovered half a century later in ion-atom collisions [22].

All the foregoing studies relate to ionization by *electron* impact. The possibility of multielectron excitation or ionization by *photon* impact was realized much more recently. As late as 1957, Sandström wrote in an authoritative monograph: "A characteristic feature of the satellites is the fact that they do not appear in the secondary radiation generated through irradiation of matter by x rays" [23]. Only in the 1960s was the subject of multiple photoexcitation broached, through calculation of the shakeoff rates in charge spectra induced by x rays in noble-gas atoms [24–26] and the development of a gen-

eral theory of x-ray satellites based on a sudden-approximation treatment of x-ray excitation [2].

Absorption spectra can, in principle, reveal multiple inner-shell photoexcitation processes by displaying concomitant changes in the total photoeffect cross section. Thus Schnopper [27] in 1963 observed features in the Ar x-ray absorption spectrum that could be traced to M-electron shake accompanying K-shell photoionization. The same year, Madden and Codling discovered doubly excited autoionizing states of He in a synchrotron-radiation absorption experiment on the National Bureau of Standards storage ring SURF [28,29]. This classic experiment had great impact upon the field as it demonstrated the powerful potential of synchrotron radiation research in atomic physics, which has been explored increasingly since that time. A striking illustration of this potential is seen, for example, if one compares Schnopper's [27] conventionally excited Ar $[KM]$ absorption spectrum [30] with that of Deslattes *et al.* [10], recorded twenty years later with synchrotron radiation; the latter spectrum shows an elaborate, clearly identifiable structure.

Double-excitation features in absorption spectra of solids are particularly elusive. Solid absorbers pose problems that arise from uneven sample thickness and, in particular, from x-ray absorption fine structure (XAFS) that is readily confused with multielectron absorption signals, unless it is differentiated on the basis of its temperature dependence [31]. Over the past decade, a number of reports has been published on $[KL]$ double absorption in transition metals [32–36], $[L^2]$ edges in lanthanides [37–39] and even $[K^2]$ in Cu [40]. In a recent systematic study with synchrotron radiation in the Hamburger Synchrotronstrahlungslabor, however, none of these "edges" could be confirmed, and in at least one case, that of Co [36], the reported feature was shown to be part of the far-XAFS structure [31]. Not until very recently has a technique been developed which allows double-excitation features in crystalline samples to be disentangled from the underlying XAFS structure [41]. The procedure is rather complicated and has so far led only to identification of the positions of a few double-excitation steps.

Even with gaseous samples, identification of inner-shell multielectron absorption features is exceedingly difficult. The very weak signals tend to be obscured by noise from various sources including photon-beam fluctuations and "glitches" produced, for example, by *umweganregung* [42] in the monochromator crystals. Nevertheless, several interesting observations have been made, in addition to those [10,27] already mentioned. Esteva *et al.* [43] detected Ne $[KL]$ double excitation to higher bound states. Si $[KL]$ features in SiF_4 absorption spectra were reported by Bodeur *et al.* [44], and in Ar spectra, by Kuetgens and Hormes [45]. Multielectron absorption features accompanying Kr K-shell ionization have been studied by Deutsch and Hart [46,47], Frahm and coworkers [31,48], Bernieri and Burattini [49], and Ito *et al.* [50]. Deutsch and Kizler [51] have recently observed several double excitation features near the K edge of Xe. Dezarnaud, Guillet, and Tronc [52] have observed double-electron excitations above the Xe $L_{2,3}$ edges in an ion-yield experiment. A theoretical study of K absorption structures of Ne, Na, and Ar in the region of double excitation or ionization has been performed by Sukhorukov *et al.* [53].

It can fairly be expected that the much higher photon flux from upcoming third-generation synchrotron-radiation sources [54] will make it possible to measure absorption spectra of multielectron inner-shell photoexcitation phenomena that currently elude detection, providing an important supplement to information on such processes gathered from x-ray and electron satellites. Noble-gas spectra being the most tractable and unequivocal, we review here the pertinent theory and derive lowest-order predictions for Kr absorption spectra. We describe a synchrotron-radiation measurement of these spectra that generally characterizes current limitations of such experiments and engage in some speculation as to the potential of future measurements of this kind.

A dependable theoretical model is necessary to serve as a guide in the interpretation of putative inner-shell multielectron excitation features in measured absorption spectra, because in many cases these structures fall near or below the limits of detectability with present-day experimental resources. In Sec. II we describe the calculation of single- and multielectron photoexcitation and ionization cross sections, with emphasis on threshold behavior. The calculation of threshold energies of doubly excited states is discussed. Quantitative predictions are derived for pertinent Kr $[1s,nl]$ absorption features superimposed upon the $[1s]$ spectra. In Sec. III, an experiment on two-electron inner-shell photoexcitation of Kr is described, and in Secs. IV and V, we compare theoretical predictions with results of the present experiment and of other measurements reported in the literature.

II. THEORY

A. Total and single-electron photoionization cross sections

Well above threshold, the theoretical subshell photoionization cross sections of Scofield [55] are quite dependable. In these calculations, the electrons were treated relativistically and assumed to be moving in the same Hartree-Slater central potential in the initial and final states. All relevant multipoles as well as retardation effects were included. Because a frozen-core potential was used, the partial cross sections effectively account for all excitation (shakeup) and ionization (shakeoff) that accompany the ejection of the photoelectron [56]. This explains the good overall agreement between Scofield's results [55] and total experimental cross sections [57,58]. The accuracy of the results has also been borne out by some systematic comparisons with measured partial L-subshell cross sections [59].

Near threshold, on the other hand, the dynamics of the excape of the photoelectron from a deep inner shell in a many-electron atom is complex [60]. It was already pointed out by Amusia, Ivanov, and Kupchenko [61] that inner-shell single-electron photoionization cross sections

can be dramatically affected by the post-collision interaction between photo- and Auger electrons in the field of the residual ion, which further complicates the picture; this phenomenon can be treated [62,63] from the point of view of resonant scattering theory [64–66], while in principle it requires a generalization of the K-matrix theory of single-electron photoionization [67], which has not yet been accomplished. Tulkki and Åberg [60] have been quite successful in treating the near-threshold K-shell photoionization of Ar by using their Dirac-Fock continuum program in conjunction with the multiconfiguration Dirac-Fock code of Grant *et al.* [68] for the calculation of various approximate relativistic K absorption cross sections. These authors took relaxation into account completely by constructing separate solutions for the ground state and the final [1s] hole state, and by including all the resulting overlap matrix elements between the initial- and final-state one-electron four-spinors in the transition amplitude. Post-collision interaction was taken into account approximately by incorporating the lowest-order scattering-theory amplitude into the cross section. Inclusion of this amplitude was found to lower the cross section at threshold by 15%. The resulting cross section was nearly gauge independent; only the $E1$ multipole was found to contribute significantly. Similar results were obtained for the Xe and Rn 1s cross sections, except that relativistic effects are more significant [69]. Agreement with existing experiments is very good for Ar [10,46,47] and Xe [51].

In the present work, the Kr 1s photoionization cross section was calculated by the same method, except that the effect of the post-collision interaction was disregarded (Table I). The 1s photoexcitation cross sections for $1s \rightarrow np_{1/2,3/2}$ transitions, $5 \leq n \leq 9$, were also calculated by including all overlap matrix elements. The quantum-defect method was used to evaluate the contribution from $n \geq 10$ states. The resulting cross sections were convoluted with a Lorentzian of width equal to the 1s natural width and the instrumental resolution function.

TABLE I. Theoretical Kr 1s photoionization cross section. The Kr 1s binding energy is taken to be 14 327.17 eV (see Ref. [101]).

Photon energy (eV)	Cross section (b)
14 327.22	16 007.70
14 332.22	15 567.60
14 337.22	15 127.00
14 342.22	14 793.80
14 347.22	14 548.50
14 367.22	14 026.90
14 392.22	13 747.20
14 422.22	13 548.20
14 527.22	13 061.00
14 627.22	12 667.50
14 727.22	12 328.00
14 827.22	12 029.80

B. Two-electron photoexcitation and ionization cross sections

Two atomic electrons can be promoted upon absorption of one photon due to the Coulombic electron-electron interaction. At photon energies below the threshold for excitations accompanying ionization, the creation of two atomic vacancies can take place with discrete two-electron excitations. With increasing photon energy, the process eventually evolves into double photoionization. Discrete steps can occur in the absorption spectrum only if a discrete excitation takes place. Double photoionization does not give rise to a step or "edge" since the corresponding cross section rises smoothly from zero as the photon energy increases above the threshold value.

Within the multichannel multiconfiguration Dirac-Fock (MMCDF) method [7,70], which is a generalization of the Dirac-Fock method referred to in Sec. II A, the correlation effects responsible for *direct* two-electron processes can be classified as follows: (i) relaxation or core rearrangement, (ii) initial-state configuration interaction, (iii) final-ionic-state configuration interaction, and (iv) final-continuum-state configuration or final-state channel interaction. This classification is a generalization of a scheme which is often used to disentangle correlation effects in ordinary Auger-electron emission spectra [70,71]. Since Auger-electron emission can be treated as a resonance in double photoionization [72], this *indirect* process including post-collision interaction is naturally incorporated in our scheme. Processes in which doubly excited inner-shell hole states decay by autoionization can be treated in an analogous fashion as resonances in the one-electron photoionization cross section. The transition amplitude of the two-electron processes in inner-shell photoionization thus consists of the sum of the direct nonresonant and the indirect resonant amplitudes, both of which are subject to correlation mechanisms of types (i)–(iv).

Mechanisms that contribute to two-electron photoionization of the outermost shells in rare-gas atoms have been separated within many-body perturbation theory [73]. In first order of the combined perturbations by the photon field and electron correlations, the important contributions are (1) core rearrangement, (2) initial-state correlations, (3) virtual Auger transitions, and (4) direct collisions. The different mechanisms have been found to be of varying importance, depending on the photon energy relative to the double-ionization threshold energy, the orbitals which are ionized, and the relative final-state energies of the electrons that undergo transitions. If treated nonperturbatively they can be considered to belong within the MMCDF scheme to categories (i)–(iv), respectively.

Shakeup and shakeoff processes correspond to core rearrangement if the initial-state orbital from which the photoelectron originates describes one of the final-state holes. In direct shakeup or shakeoff accompanying photoionization, an orbital electron undergoes an electric monopole ($E0$) transition into an excited state or into the continuum while the photoelectron is emitted through an

electric dipole ($E1$) transition; in conjugate shake processes, the $E0$ and $E1$ roles are reversed. In either case, the photoelectron energy is diminished accordingly. In general, conjugate shake processes tend to contribute negligibly, except near the threshold [60,74]. For example, Krause and Caldwell [15] found that conjugate shakeup to final $1s(2s2p\ ^{1,3}P)$ states of Be contributes fully 40% as much as single ionization at threshold.

Contributions of shake processes can be studied by solving for the initial and final states separately and calculating the matrix elements of the photon-electron interaction operator between these states [4,75]. In principle, all nonorthogonal overlap elements between the single-electron states must be included in calculating the cross sections. If the photon energy is sufficiently high above threshold, the sudden approximation can be used to determine the distribution of shakeup and shakeoff states relative to the one-electron process [2]. In this approximation, the photoelectron is taken to leave the atom so quickly that the remaining atomic electrons redistribute themselves into an eigenstate of the new Hamiltonian, in accordance with the overlaps of the parent frozen-core one-hole wave function with eigenfunctions of the daughter atom. At high photon energies, the shakeoff and shakeup populations relative to the one-hole final-state population therefore become energy independent. A recent experiment in which electron spectra from photoionization and nuclear internal conversion were compared has confirmed the validity of this picture [76].

The effect of initial-state and final-ionic-state correlation on double photoexcitation can be gauged by employing multiconfiguration wave functions. By this means, it has been shown that the high correlation of valence electrons significantly affects the shakeup distribution of $2p$ electrons accompanying $1s$ photoionization of Ne in the sudden-approximation regime [77]. The final-ionic-state and final-continuum-state configuration interactions, including direct collisions and virtual Auger transitions, were found to contribute significantly to the multiple excitation processes near the Xe $5s$ threshold [7].

In the present treatment of double photoexcitation and ionization of Kr, the initial and final bound-state orbitals were optimized separately. In the calculation of photon-electron interaction matrix elements for ionization accompanied by excitation to bound states, the excited orbital was generated in the potential of the final ionic core with two holes, whereas the continuum orbital was calculated in the combined field of the core and the excited electron. To find double-ionization amplitudes, both continuum orbitals were calculated in the field of the double-hole core. The bound- and continuum-state orbitals were used for the construction of the Slater determinants from which the initial- and final-state many-electron wave functions of proper symmetry could be obtained for each particular $1s$ photoionization process. Of the different mechanisms for double excitation described earlier, this method includes only shakeup and shakeoff. Cross sections for double photoexcitations to Kr $[1s4p]$, $[1s3d]$, and $[1s3p]$ final states were calculated with Hartree-Fock bound- [78] and continuum-state orbitals [79]. In calculating excitations to $[1sns]$ final states with these wave functions, however, off-diagonal contributions were found to dominate the cross sections because of large $\langle ns|n's\rangle$ overlap elements between initial and final states. This unphysical feature is a consequence of the breakdown of the orthogonalization procedure for bound Hartree-Fock orbitals when the configuration has two open subshells of the same symmetry and occupancy. With relativistic Dirac-Fock wave functions [68], on the other hand, complete orthogonality was achieved for the $[1s2s]J=1$ state. We therefore employed the MMCDF method [7,70] in the single-configuration, single-channel, atomic-state mode for the calculation of the $[1s2s]$ cross sections.

1. Hartree-Fock calculations: $[1s4p]$, $[1s3d]$ and $[1s3p]$ final states

Within the dipole approximation, the cross section for photoionization at photon energy ω is

$$\sigma(\omega)=4\pi^2\alpha\omega\sum_f\left|\left\langle\Psi_i\left|\hat{\varepsilon}\cdot\sum_{j=1}^{N}\mathbf{r}_j\right|\Psi_f\right\rangle\right|^2\delta(\omega+E_i-E_f)\ , \tag{1}$$

where Ψ_i is the initial many-electron ground-state wave function of energy E_i and Ψ_f is one of the possible final-state wave functions of energy E_f. Equation (1) is expressed in atomic units, with respect to the unit polarization vector $\hat{\varepsilon}$. The dipole matrix element between many-electron determinantal initial- and final-state wave functions was calculated according to the method described by Löwdin [80]. For a pair of single-determinantal wave functions the relevant formula is

$$\left\langle\Psi_i\left|\sum_{j=1}^{N}\mathbf{r}_j\right|\Psi_f\right\rangle=\sum_{kl}\langle k|\mathbf{r}|l\rangle D_{\Psi_i\Psi_f}(k|l)\ , \tag{2}$$

where k and l are single-electron initial- and final-state orbitals and $D_{\Psi_i\Psi_f}(k|l)$ is the minor of the overlap determinant between Ψ_i and Ψ_f in which row k and column l have been removed.

Final-state calculations can be divided into three categories, depending on the photon energy relative to the double-ionization threshold and on the relative energies of the photoelectron and shaken electron: (i) bound-bound states in which both the photo- and shaken electrons are bound to the core, (ii) bound-continuum states in which one of the electrons is in the continuum and the other electron is bound to the core, and (iii) continuum-continuum states in which both electrons are in the continuum. In calculating the bound-bound states, the interaction between the photo- and shaken electron was included by solving for the two electrons simultaneously outside the two-hole frozen core. Bound-continuum states were calculated by first solving for the bound electron outside the frozen core and then the continuum elec-

tron outside this singly ionized excited state. The frozen-core orbitals were generated using the Hartree-Fock configuration-average scheme [78]. These orbitals were then used in the construction of an average Hartree-Fock potential for the electrons outside the core, with the exchange interaction taken into account. Continuum-continuum states were calculated by solving for the positive-energy orbitals separately outside the frozen core, using a code developed by Armen [79,81]; the interaction between the continuum electrons was not taken into account.

For example, in the case of two-electron excitation in which the $3d$ electron is shaken off and the $1s$ electron undergoes a dipole or a combined monopole-dipole transition into the continuum, the matrix element in Eq. (1) becomes

$$\left\langle \Psi_0 \left| \hat{\epsilon}\cdot\sum_{j=1}^{N}\mathbf{r}_j \right| \Psi_{[1s3d]\epsilon p\epsilon' d} \right\rangle = \sum_{ns} \langle ns|z|\epsilon p\rangle D_{\Psi_0\Psi_{[1s3d]\epsilon p\epsilon' d}}(ns|\epsilon p)\ , \quad (3)$$

if terms with double- and triple-order products of overlap elements $\langle n_i|n_f\rangle$ $(n_i\neq n_f, l>0)$, including amplitudes for conjugate shake processes, are neglected. In Eq. (3), we have $z=\hat{\epsilon}\cdot\mathbf{r}$, Ψ_0 is the ^1S ground-state wave function of a closed-shell atom, and $\Psi_{[1s3d]\epsilon p\epsilon' d}$ is an uncoupled single-determinantal wave function for the final state, with holes in the $1s$ and $3d$ orbitals and continuum electrons ϵp and $\epsilon' d$. The sum over ns only includes the occupied ground-state s orbitals. A full determinant in this case can be written

$$\begin{array}{c|cccccccccccc}
 & \epsilon p_0^+ & 1s^- & 2s^+ & \cdots & 3p_{+1}^- & \cdots & 4p_0^+ & \cdots & 4p_{+1}^- & \epsilon' d_{-2}^+ & 3d_{-2}^- & \cdots \\
1s^+ & 0 & 0 & \langle 1s|2s\rangle & \cdots & 0 & \cdots & 0 & \cdots & 0 & 0 & 0 & \cdots \\
1s^- & 0 & \langle 1s|1s\rangle & 0 & \cdots & 0 & \cdots & 0 & \cdots & 0 & 0 & 0 & \cdots \\
2s^+ & 0 & 0 & \langle 2s|2s\rangle & \cdots & 0 & \cdots & 0 & \cdots & 0 & 0 & 0 & \cdots \\
\vdots & & & & \ddots & & & & & & & & \\
3p_{+1}^- & 0 & 0 & 0 & \cdots & \langle 3p|3p\rangle & \cdots & 0 & \cdots & \langle 3p|4p\rangle & 0 & 0 & \cdots \\
\vdots & & & & & & \ddots & & & & & & \\
4p_0^+ & \langle 4p|\epsilon p\rangle & 0 & 0 & \cdots & 0 & \cdots & \langle 4p|4p\rangle & \cdots & 0 & 0 & 0 & \cdots \\
\vdots & & & & & & & & \ddots & & & & \\
4p_{+1}^- & 0 & 0 & 0 & \cdots & \langle 4p|3p\rangle & \cdots & 0 & \cdots & \langle 4p|4p\rangle & 0 & 0 & \cdots \\
3d_{-2}^+ & 0 & 0 & 0 & \cdots & 0 & \cdots & 0 & \cdots & 0 & \langle 3d|\epsilon' d\rangle & 0 & \cdots \\
3d_{-2}^- & 0 & 0 & 0 & \cdots & 0 & \cdots & 0 & \cdots & 0 & 0 & \langle 3d|3d\rangle & \cdots \\
\vdots & & & & & & & & & & & & \ddots
\end{array} \quad (4)$$

The total cross section for $3d$ shake then becomes the sum over four partial cross sections corresponding to final states in which (i) both electrons are bound to the double-hole core, (ii) the $1s$ electron is bound to the core and the $3d$ electron is in the continuum, (iii) the $1s$ electron is in the continuum and the $3d$ electron is bound to the core, and (iv) both electrons are in the continuum.

The cross sections for transitions to doubly excited $[1s3d]\bar{n}pn'd$ states can be written

$$\sigma_{bb}(\omega)=\frac{4\pi^2\alpha}{3}\omega q_{1s}q_{3d}\times\left[\sum_{ns}\langle ns|r|\bar{n}p\rangle D_{\Psi_0\Psi_{[1s3d]\bar{n}pn'd}}(ns|\bar{n}p)\right]^2\times\delta(\omega-E_{\rm exc}([1s3d]\bar{n}pn'd))\ , \quad (5)$$

where q_{nl} is the ground-state occupation number for orbital nl and $E_{\rm exc}$ is the excitation energy of the doubly excited state. In Eq. (5), $\langle ns|r|\bar{n}p\rangle$ is the radial dipole matrix element between the initial ns and final $\bar{n}p$ orbitals. The excitation energies were calculated by adding to the double-ionization threshold Dirac-Fock energies the differences between Hartree-Fock doubly ionized state energies and frozen-core excited-state energies (see Sec. II C). Bound-bound transitions were summed over np and $n'd$ orbitals for $n=5-12$ and $n'=4-11$. The case of transitions to doubly excited $[1snp]\bar{n}pn'p$ $(n=3,4)$ states was treated using a formula similar to Eq. (5) except that q_{3d} was replaced by q_{np}. The sum over the $n'p$ shakeup states included $n'=5-12$.

For transitions to final states with the $1s$ electron bound to the core and the $3d$ electron in the continuum, the partial cross section per unit energy is

$$\frac{d\sigma_{bc}(\omega)}{d\epsilon}=\frac{4\pi^2\alpha}{3}\omega q_{1s}q_{3d}\times\left[\sum_{ns}\langle ns|r|n'p\rangle D_{\Psi_0\Psi[1s3d]n'p\epsilon d}(ns|n'p)\right]^2\times\delta(\omega-\epsilon-E_{\rm exc}([1s3d]n'p))\ , \quad (6)$$

in which ϵ is the energy of the d electron. Cross sections for the first eight Rydberg $n'p$ states were calculated by solving for the $n'p$ wave function outside the double-hole core and calculating the corresponding matrix elements. To include the contributions of higher Rydberg orbitals,

the $n'=11$ and 12 wave functions were used to determine the parameters A and δ in the empirical quantum-defect relation [82]

$$|\langle ns|r|n'p\rangle|^2=\frac{A}{(n'-\delta)^3} . \tag{7}$$

Cross sections σ_{cb}, for transitions to final states with the $1s$ electron in the continuum and the $3d$ electron in a bound state, can be described by replacing the state $n'p$ in Eq. (6) with ϵp and the state ϵd with $n'd$.

The partial doubly differential cross section for shake-off transitions in which both electrons make transitions to the continuum can be written

$$\frac{d^2\sigma_{cc}(\omega)}{d\epsilon d\epsilon'}=\frac{4\pi^2\alpha}{3}\omega q_{1s}q_{3d} \times\left[\sum_{ns}\langle ns|r|\epsilon p\rangle D_{\Psi_0\Psi_{[1s3d]\epsilon p\epsilon' d}}(ns|\epsilon p)\right]^2 \times\delta(\omega-\epsilon-\epsilon'-E_B^{++}) , \tag{8}$$

where E_B^{++} is the threshold energy for double ionization.

In cases of shake from an np orbital accompanying the dipole transition of a $1s$ electron, the cross-section formula must include exchange matrix elements. If the $1s$ electron undergoes a dipole transition to an ϵp state and the np electron is shaken off into an $\epsilon' p$ state, there will be exchange matrix elements between the $1s$ and $\epsilon' p$ orbitals and between the np and ϵp orbitals. We have used the cross-section formula [4]

$$\frac{d^2\sigma}{d\epsilon d\epsilon'}=\frac{4\pi^2\alpha}{3}\omega[5A_+(\epsilon)^2+7A_-(\epsilon)]^2 \times\delta(\omega-\epsilon-\epsilon'-E_B^{++}) , \tag{9}$$

where, in this case,

$$A_\pm(\epsilon)=\sum_{ns}\langle ns|r|\epsilon p\rangle D_{\Psi_0\Psi_{[1snp]\epsilon p\epsilon' p}}(ns|\epsilon p) \pm\sum_{ns}\langle ns|r|\epsilon' p\rangle D_{\Psi_0\Psi_{[1snp]\epsilon p\epsilon' p}}(ns|\epsilon' p) . \tag{10}$$

The cross-section formulas (5), (6), (8), and (9) do not account for the final-state lifetime broadening. The lifetime can be taken into account by replacing the Dirac delta function $\delta(x)$ by the normalized Lorentzian density function $\Gamma/2\pi(x^2+\Gamma^2/4)$ with x standing for the appropriate energy differences in these equations. The width Γ is the sum of the widths Γ_{1s} and Γ_{nl} of the two holes involved in the final $[1snl]$ core-hole states. The total ionization cross sections are then obtained by integrating over ϵ in Eq. (6) and over ϵ and ϵ' in Eqs. (8) and (9). In the integration over the double-ionization continuum, each pair of energies ϵ and ϵ' must be counted only once. The resulting cross sections were also convoluted with the instrumental resolution function.

2. *Dirac-Fock calculations: [1s2s] and [1s2s4p] final states*

In the present calculations of $[1s2s]$ and $[1s2s4p]$ excitations we make use of the relativistic electric dipole photoionization cross section of Tulkki *et al.* [60,62]. The cross section for production of the triply excited $[1s2s4p]$ final state was calculated as well in order to investigate a discrepancy between theory and experiment in the $[1s2s]$ threshold region (Sec. IV B 4). Wave functions and eigenenergies were calculated by the single-channel, single-configuration Dirac-Fock method. The Coulomb gauge was employed. Initial and final bound-state orbitals were calculated separately and all overlap integrals were included in the many-electron $E1$ transition amplitudes. The excited and continuum-state orbitals were calculated in the field of the double-hole core in the same manner as the Hartree-Fock wave functions (Sec. II B 1). Excitations to high Rydberg states were included through use of the quantum-defect method, as discussed above (Sec. II B 1). Upper and lower limits of the double-shake probability were estimated through statistical arguments [4]. The only quantity needed is the square of the overlap matrix element between the corresponding ground- and final-state orbitals with the same quantum numbers. Calculations of the final two- and three-hole states then lead to the double-shake probability limits. Lagrangian multipliers were included in all calculations in order to obtain a strictly orthogonal set of final-state orbitals for the $[1s2s]J=1$ state.

C. Energies of multiply excited states

1. *Self-consistent-field calculations*

Excited-state threshold energies were evaluated as differences between the total energies of the excited ionic states and of the ground state, calculated by separate self-consistent-field (SCF) procedures. This $\Delta E_{\rm SCF}$ method takes account of full relaxation [83].

Zeroth-order wave functions and energies were computed in terms of relativistic independent-particle models. Two approaches were used. In the first one, Liberman's version [84] of the Dirac-Hartree-Slater method was used with a modified finite-nucleus routine. A first-order correction to the local approximation was made by computing the expectation of the total Hamiltonian with zeroth-order wave functions [85–87]. The Breit interaction was taken into account by including the frequency-dependent Breit operator [88] in the Hamiltonian, thus incorporating the magnetic and retardation contributions to the binding energies in the SCF approach [89].

Self-energy and vacuum polarization, the two main radiative corrections from quantum electrodynamics (QED), were included in the energy calculations. Self-energy corrections for K and L levels were calculated from point-Coulomb values [90] with an effective-charge screening procedure [87]; for M_1, $M_{2,3}$, and N_1 levels, the self-energy corrections were estimated by the n^{-3} scaling rule and effective-charge approach [89]. The vacuum-polarization shift was included perturbatively by using the Uehling potential and higher-order terms according to Huang [91,86,87].

In a second approach, relativistic SCF energies were calculated with the multi-configuration Dirac-Fock (MCDF) code of Grant *et al.* [68]; details are given by Chen [92]. Test comparisons were made with results obtained with the modernized version of the Oxford MCDF

code, GRASP-2 [93]. Energies calculated by the three different SCF approaches were found to agree to within 1 eV in all cases.

In addition to relativistic and QED contributions, accurate atomic energy-level calculations must include the shifts caused by correlation effects [72,89]. Leading factors among these are ground-state correlation and interaction between the discrete hole state and the continuum. The ground-state correlation correction arises because of pair correlations lost upon ionization [94]. Ground-state correlation shifts were included in the present calculations, as were discrete-continuum level shifts [95–97] of $1s$ and $2s$ binding energies.

The calculated energies of pertinent excited states are listed in Table II. For comparison purposes, some results are listed not only for Kr but also for Xe.

2. *Splitting of* [*ns,n's*] *states*

An interesting result is the prediction of an effect that arises exclusively from the relativistic Breit-Coulomb Hamiltonian [98], viz. the splitting of excitations that comprise two vacancies in s states into distinct ^1S and ^3S levels. This splitting contains a dominant contribution from the spin dependence of the relativistic Coulomb interaction and a smaller contribution from the Breit operator.

We illustrate the effect by calculating the splitting between the $[1s2s]\,^3S_1$ and $[1s2s]\,^1S_0$ double-hole states. Including only the Coulomb interaction, we have

$$\begin{aligned} E(^3S_1) &= E_{\rm av} - \tfrac{1}{2}G^0(1s2s)\ , \\ E(^1S_0) &= E_{\rm av} + \tfrac{3}{2}G^0(1s2s)\ , \\ \Delta E(^1S_0 - ^3S_1) &= 2G^0(1s2s)\ , \end{aligned} \tag{11}$$

where $G^0(1s2s)$ is the Coulomb-interaction exchange integral.

Specifically, for the Kr $[1s2s]$ double-vacancy state we find $\Delta E(^1S_0 - ^3S_1)_{\rm Coulomb} = 40.12$ eV and $\Delta E(^1S_0 - ^3S_1)_{\rm Coulomb+Breit} = 43.00$ eV, i.e., the Breit interaction enhances the splitting by 6.7% in this case. For the Xe $[2s3s]$ state, we calculate $\Delta E(^1S_0 - ^3S_1)_{\rm Coulomb} = 17.6$ eV and $\Delta E(^1S_0 - ^3S_1)_{\rm Coulomb+Breit} = 17.9$ eV.

III. EXPERIMENT

An experiment to search for absorption features due to double inner-shell excitation in Kr was performed on bending-magnet beamline III-2 in the Stanford Synchrotron Radiation Laboratory. A narrow x-ray energy band was selected from hard radiation emitted by ~3-GeV electrons in the SPEAR ring by means of a Bragg-diffraction monochromator that contained two Si crystals in the $(n, -n)$ position, reflecting from (220) planes. The full energy width at half maximum of the monochromatized x-ray beam was ~1.6 eV at 14.0 keV of which the Darwin width contributed 0.84 eV, the remainder being due to beam divergence defined by an 0.025-cm-high entrance slit. The apparatus has been described earlier in more detail [101]. The x-ray beam traversed a 15.2-cm-long upstream ion chamber producing a current I_0, the sample chamber, and a 30.5-cm-long downstream ion chamber delivering current I_1. The currents from the ion chambers were converted to voltages in Keithley 427 electrometers that had been selected for low noise. The voltage signals drove two voltage-controlled oscillators the output frequencies of which were measured by a dual-gated scaler interfaced with a computer.

The search for the $1s2s$ double-hole features requires that noise be kept more than four orders of magnitude below the K jump, calling for special precautions. To attain this aim, the sample cells were chosen somewhat smaller than two absorption lengths [99]. Noise due to jitter in the vertical position of the circulating electron beam in SPEAR was found to exceed Poisson noise by at least a factor of 2. The noise produced by this jitter was halved by detuning the second monochromator crystal to ~0.7 of the rocking-curve maximum; this measure also effectively suppressed higher-order diffraction harmonics [100]. The absorption cell was filled to 1 atm pressure with 99.995% pure Kr. The I_0 and I_1 ion chambers were filled with Ar, both to 1 atm. Chamber windows were made of 6-μm Kapton or 0.13-mm Be.

The energy scale of the double-crystal monochromator was calibrated through measurements of the Kr K edge [101] and the Th L_3 edge [102]. Additional calibration points were derived from the well-resolved $1s4p$ double-absorption structure of Kr [46]. The energy stability was better than $< \pm 1.3$ eV throughout the duration of the experiments. This variation in energy corresponds to changes in the vertical position of the electron beam in the storage ring by $< \pm 0.4$ mm.

Absorption spectra were measured by scanning regions of ≥ 100 eV centered on the calculated energies of the Kr $[1s4p]$, $[1s3d]$, $[1s3p]$, and $[1s2s]$ double-hole states. For each measurement, 10–15 scans were performed in 1-eV steps with 1-s dwell time; a 1-s instrumental relaxation pause was allowed between steps. During each typical 1-s counting period, of the order of 10^9 photons were absorbed in each chamber and in the absorption cell. Control scans of the same duration with air-filled absorption cells were carried out to check for systematic artifacts.

IV. RESULTS AND DISCUSSION

Measurements of multiple inner-shell photoexcitation features in absorption spectra are encumbered by two factors. (1) The pertinent double-excitation cross sections are generally 3 to 4 orders of magnitude smaller than single-photoionization cross sections at the same photon energy. (2) Reasonably sharp, edgelike absorption profiles are produced only if promotion of one electron to the continuum is accompanied by shakeup of the second electron to a bound state; if both electrons undergo transitions to the continuum, then the onset of the cross section for the two-electron process tends to be gradual with photon energy, without sharp, readily recognizable features [4,9]. For more tightly bound inner-shell electrons, absorption into shakeoff states increasingly dom-

inates over shakeup, as noted in sudden-approximation calculations [103], whence double-excitation edges are suppressed and the total probability of two-electron processes becomes more difficult to detect.

It follows that interpretation of the absorption spectra hinges crucially on estimation of the single-electron photoionization components that underly the multiexcitation features. In the present work, a third-order polynomial was fitted to the measured absorption spectra in the photon-energy region below the calculated threshold energy for the double-electron excitations. The polynomial was further constrained, ≥ 200 eV above the threshold, to join smoothly onto the measured absorption cross section from which the calculated double-electron cross section had been subtracted; the criterion for smoothness was matching of the first derivative with respect to photon energy. Only for $1s2s$ excitations, which were the most difficult to detect, the underlying components were subtracted by fitting a function

$$f(\varepsilon)=\sigma_{L,M,N}(\varepsilon)+a\sigma_{1s}(\varepsilon)+b+c\varepsilon \quad (12)$$

to the absorption spectrum below the calculated threshold energy. Here, $\sigma_{L,M,N}$ and σ_{1s} are the theoretical cross sections discussed in Sec. II A, ε is the photon energy, and a, b, and c are fitting parameters.

The experimental cross-section scale was normalized at a photon energy of 14 400 eV by reference to the Kr K-edge cross section measured by Deutsch and Hart [104] as shown in Fig. 1. The present measurement and that of Ref. [104] agree well but for slight differences in the photon-energy regions below and far above the K edge. The theoretical total cross section, also shown in Fig. 1, is the sum of the partial one-electron ionization cross sections σ_{1s} (not including bound-bound transitions) and $\sigma_{L,M,N}$ (Sec. II A) and the double-electron excitation cross sections discussed in Sec. II B. As stated above, theoretical cross sections were convoluted with (1) a Lorentzian of width equal to Γ_{1s} or $\Gamma_{1s}+\Gamma_{nl}$ [105], depending upon the excitation involved, and (2) a Gaussian of 1.6-eV full width at half maximum to account for the energy width of the incident x-ray beam. In the remainder of this section, theoretical and measured cross sections are compared.

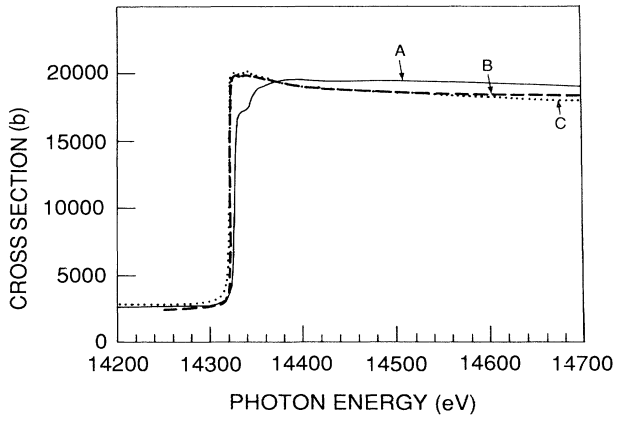

FIG. 1. X-ray absorption cross section near the Kr K edge: A, theoretical total cross section (present work); B, measurement by Deutsch and Hart (Ref. [104]); C, present measurement.

A. Total photon absorption cross section above the Kr K edge

The measured total absorption cross section is compared in Fig. 2(a) with theoretical partial and total cross sections. In the region between the Kr $1s$ binding energy (14 327.2 eV [101]) and the $1s4p$ double-ionization threshold at 14 353 eV (Table II), the theoretical cross section falls below the experimental curve. Taking account of the fact that the sum of theoretical higher-shell cross sections $\sigma_{L,M,N}$ [55] falls 9% below the experimental cross sections well below the K edge, and subtracting the small contributions from $[1s4p]npn'p$ excitations discussed below in Sec. IV B 1, the theoretical single $1s$ absorption cross section without inclusion of bound-bound

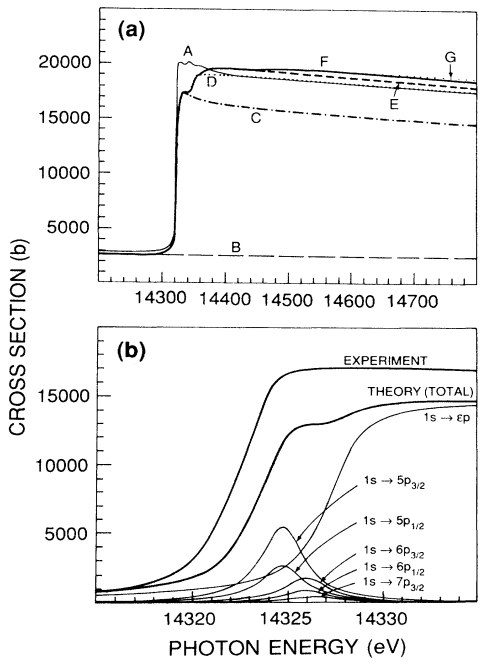

FIG. 2. (a) A, measured x-ray absorption cross section of Kr near the K edge; B, calculated cross section for photoionization of higher (L, M, and N) shells (Ref. [55]); C, theoretical $1s$ photoionization and bound-bound excitation cross section plus higher-shell contributions as indicated by curve B; D, calculated $1s4p$ two-electron excitation cross section added to curve C; E, curve D with calculated $1s4s$-excitation cross section added; F, curve E with calculated $1s3d$ excitations added; G, curve F with calculated $1s3p$ excitations added. (b) Expanded graph of the Kr K-edge region. EXPERIMENT, measured K absorption cross section, with $\sigma_{L,M,N}$ according to Ref. [51] subtracted. THEORY (TOTAL), calculated total absorption, including ionization and transitions to np_j states ($5 \leq n \leq 9$), convoluted with a 1.6-eV-wide Gaussian instrumental resolution function. Calculated $1s \rightarrow np_j$ ($5 \leq n \leq 7$) transition probabilities are also indicated, without instrumental resolution correction.

TABLE II. Theoretical energies of double-hole states (in eV).

State	$\Delta E(^1S_0\text{-}^3S_1)$ Coulomb	$\Delta E(^1S_0\text{-}^3S_1)$ Coulomb plus Breit	Average binding energy[a] (1)[b]	Average binding energy[a] (2)[c]
		Krypton		
$[1s2s]$	40.12	43.00		
$[1s2s]\,^3S5s$				16 343
$[1s2s]\,^3S$			16 360	16 353
$[1s2s]\,^3S[4p_{3/2}]5s5p_{3/2}$			16 374	16 370
$[1s2s]\,^3S[4p_{1/2}]5s5p_{1/2}$			16 375	16 371
$[1s2s]\,^3S[4p_{3/2}]5s$			16 383	16 379
$[1s2s]\,^3S[4p_{3/2}]5p_{3/2}$			16 386	16 382
$[1s3p_{3/2}]$			14 580	
$[1s3p_{1/2}]$			14 590	
$[1s3d_{5/2}]$			14 450	
$[1s3d_{3/2}]$			14 452	
$[1s4p_{1/2}]$			16 354	
$[1s4p_{3/2}]$			16 353	
		Xenon		
$[2s3s]$	17.6	17.9		
$[2s3s]\,^3S6s$			6 652	6 643
$[2s3s]\,^3S$			6 661	6 652
$[2s3s]\,^3S[5p_{3/2}]6s6p_{3/2}$			6 672	6 663
$[2s3s]\,^3S[5p_{3/2}]6p_{3/2}$			6 683	6 674

[a]Energies averaged over the 4-eV-wide multiplet splittings of the $[np](n+1)s(n+1)p$ outer open-shell states.

[b]Results from Dirac-Hartree-Slater or Dirac-Fock calculations including quantum-electrodynamic corrections and Breit energy.

[c]Same as column (1), but also including ground-state correlation and the discrete-continuum level shift of the $1s$ and $2s$ binding energies.

excitations is found to be $16.7\pm1.0\%$ smaller than the measured cross section at 14 336 eV. A disparity near the edge persists even after excitations of the $1s$ electron to bound states are included in the theory (Sec. II A), as shown in Fig. 2(b). At higher energies, with the accumulation of multielectron excitations, the total theoretical cross section from the present work begins to exceed the present measurements; at 14 800 eV, theory overestimates the data by 7.1%.

Relativistic theoretical $1s$ photoionization cross sections computed with Dirac-Fock wave functions and including complete relaxation, similar to those of the present work (Sec. II A), have been found to underestimate Ar [60] and Xe [69,106] photoabsorption as well above the K edge; in the energy region below the Ar $1s3p$ excitations, the theory was found to fall $\sim 8\%$ below the experimental cross section [60]. A substantial discrepancy in the same direction is observed with cross sections calculated from a simple hydrogenic model, with Slater-type screening constants derived from comparisons with Dirac-Fock mean radii, for both Kr [104] and Xe [106].

The total shake probability from the Kr $4p$, $4s$, $3d$, and $3p$ orbitals, relative to the $1s$ photoionization cross section, is expected to become largely independent of photon energy above $\simeq 14\,800$ eV. In fact, Table III shows that the calculated relative shake probability increases only from 34.2% at 14 800 eV to 35.9% at 15 225 eV. The latter prediction compares favorably with the result of a recent measurement of the Kr $1s$ photoelectron spectrum, which showed that the total relative probability of shake from these orbitals is $36.8\pm1.8\%$ at 15 225 eV [76]. A comparison between the present Hartree-Fock double-electron excitation cross sections and results from a Dirac-Fock calculation by Tulkki for 15 225-eV photons [76] is also included in Table III; agreement between the relativistic and nonrelativistic calculations is seen to be very good. In the Dirac-Fock calculations, the upper and lower limits of the relative probability for double shake from the N shell as described in Sec. II B 2, relative to single $1s$ ionization, were found to be 9.3% and 5.1%, respectively.

B. Multielectron excitations

1. *Kr* [*1s4p*]

The $1s4p$ absorption cross section exhibits a prominent resonance structure due to excitation of $[1s4p]npn'p$ states (Fig. 3). Above these resonances, beginning at a photon energy of $14\,350\pm2$ eV, the double-electron cross section rises as $[1s4p]\epsilon p\epsilon' p$ shakeoff states become accessible. The resonances reach a peak at $14\,342\pm1.3$ eV, in agreement with earlier reports on this structure [46,49]. The magnitude of the cross-section jump at the $1s4p$

TABLE III. Theoretical nonrelativistic (Hartree-Fock) and relativistic (Dirac-Fock) Kr double-excitation cross sections, in percent of the 1*s* ionization cross section,[a] at photon energies 14 800 and 15 225 eV.

	$\hbar\omega = 14\,800$ eV	$\hbar\omega = 15\,225$ eV	
Final state	HF	HF	DF
$[1s4p]5p\epsilon p$	12.3	12.8	13.0
$[1s4p]6p\epsilon p$	2.3	2.4	2.4
$[1s4p]7p\epsilon p$	0.9	0.9	0.9
$[1s4p]np\epsilon p$[b]	1.9	1.8	1.8
$[1s4p]\epsilon' p\epsilon p$	6.9	7.2	7.3
Total 4*p* shake	24.2	25.2	25.4
$[1s4s]5s\epsilon p$	1.9	2.0	2.0
$[1s4s]6s\epsilon p$	0.3	0.4	0.4
$[1s4s]7s\epsilon p$	0.1	0.1	0.1
$[1s4s]ns\epsilon p$[b]	0.1	0.1	0.1
$[1s4s]\epsilon' s\epsilon p$	1.3	1.4	1.4
Total 4*s* shake	3.7	3.9	4.0
$[1s3d]4d\text{-}nd\epsilon p$[c]	1.4	1.5	1.3
$[1s3d]\epsilon' d\epsilon p$	3.7	4.1	4.0
Total 3*d* shake	5.1	5.5	5.3
$[1s3p]4p\text{-}np\epsilon p$[c]	0.2	0.2	0.1
$[1s3p]\epsilon' p\epsilon p$	0.8	1.2	1.0
Total 3*p* shake	1.0	1.3	1.1
Total shakeoff	12.7	13.8	13.7
Total shakeup	21.5	22.1	22.3
Total shake	34.2	35.9	36.0

[a]The single 1*s* ionization cross section, as calculated in this work, is 12 104 b at 14 800-eV and 11 070 b at 15 225-eV photon energy.

[b]Sums over Rydberg-series members were estimated by the quantum-defect method.

[c]Total shakeup cross section.

edge, however, is found to be 460±50 b in the present work (Fig. 3), as against 383±35 b reported earlier [47]; the discrepancy may be due to different methods of subtracting the underlying contributions. In determining the fit to the single 1*s* photoionization cross section, the proximity of the *K* edge to the $1s4p$ threshold and the strong two-electron excitations required that $1s4p$ absorption be subtracted. To determine the polynomial fit, iterative estimates of the two-electron cross sections were made.

The theoretical shakeup cross section near threshold rises far above the measurements (Fig. 3). Similar excesses of theory over experiment have been found, in 1*s* excitation, for Ar 3*p* shakeup near threshold [9] and for Ne 2*p*[5,77,107] and Kr 4*p*[76] shakeup far above threshold. In the present case, the discrepancy amounts to a factor of ~4: the calculated $1s4p$ shakeup cross section reaches 2040 b at 14 357-eV photon energy. This large discrepancy between theory and experiment may be due in part to uncertainties in the single 1*s*-electron absorption in this near-threshold region. It may be possible to improve agreement of the theory by using a multiconfiguration basis set, since correlation among valence electrons is significant. In a multiconfiguration calculation of Ar $1s3p$ excitations, transitions to a $[1s3p]3d^2$ final state were found to dominate over those to the $[1s3p]4p^2$ final state [108]. An analogous transition leaving Kr in a $[1s4p]4d^2$ final state might also have a large oscillator strength.

2. *Kr [1s3d]*

Below the Kr $1s3d$ excitation threshold, the total absorption cross section depends almost linearly on photon energy. The onset of these excitations is therefore easy to detect and a fit to the underlying components can readily be made. The measured $1s3d$ excitation cross section is compared in Fig. 4 with calculated partial and total cross sections. The onset of the $1s3d$ transitions occurs at 14 423±2 eV, at a lower energy but within 7 eV of previous observations [46,49]. The measured energies of the 3*d* bound-bound excitations agree well with the present

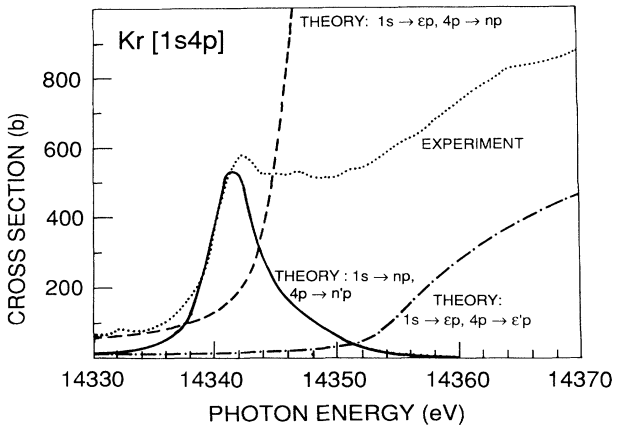

FIG. 3. Measured Kr $1s4p$ double-photoexcitation cross section (dotted curve), compared with calculated double bound-bound transitions cross section (solid curve), calculated 4*p* shakeup transitions (dashed curve), and calculated 4*p* shakeoff transitions (dash-dotted curve).

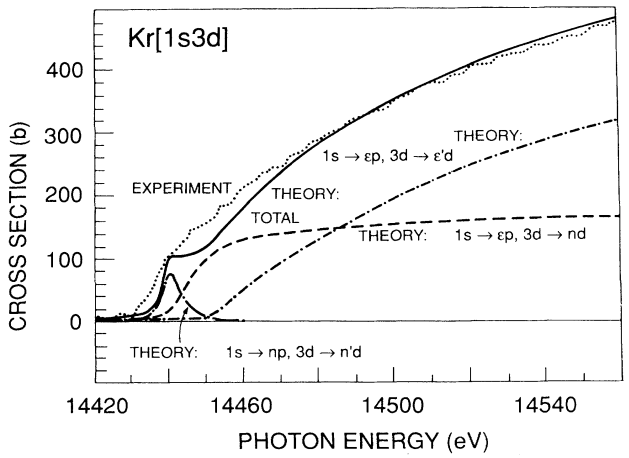

FIG. 4. Measured Kr $1s3d$ double-photoexcitation cross section (dotted curve), compared with theoretical partial and total cross sections: double bound-bound transitions (dots and long dashes), 3*d* shakeup transitions (dashed curve), 3*d* shakeoff transitions (dash-dotted curve), and the sum of calculated partial cross sections (solid curve). The very small $1s \rightarrow np, 3d \rightarrow \varepsilon d$ cross section is represented by the thin solid line.

relativistic calculations (Table II). Theory predicts levelling off of the total absorption cross section at 14 442±2 eV, as the bound-bound cross section subsides and the shakeup cross section rises with photon energy; this feature is not apparent in the data. The observed rise in cross section to 165±25 b at 14 452 eV is 4.9±1.3 times larger than previously reported [46]. As indicated in Fig. 4, transitions in which the $1s$ electron remains bound to the ion and the $3d$ electron is shaken off into the continuum are not predicted to contribute significantly to the two-electron absorption cross section. Far above threshold, the observed rise in total cross section is in good accord with the calculated rise in the shakeoff cross section. Theory indicates that, as the sudden-approximation regime is approached, the shakeoff probability exceeds that for shakeup by a factor of 3.1 (cf. Table III).

3. *Kr* [*1s3p*]

Measured and calculated cross sections for $1s3p$ photoabsorption are shown in Fig. 5. In the calculations, the spin-orbit splitting of the $3p$ level was taken into account by computing the $[1s3p_{1/2}]$ and $[1s3p_{3/2}]$ energies separately and weighing them by subshell occupation in the cross-section formulas [Eqs. (5), (6), and (8)]. The calculated splitting is 10.5 eV.

The total $1s3p$ two-electron excitation cross section is seen to rise much more gradually with photon energy than the $1s3d$ cross section. The strength of the two-electron transitions appears to be underestimated by the $[1s3p]npn'p$ bound-bound calculations. The profile of the measured $1s3p$ cross section (which exhibits considerable fluctuations due to beam jitter and statistics) qualitatively agrees with the theoretical calculation; however, the observed rise in shakeoff is slightly steeper than calculated. As in the $1s3d$ case, the probability for shakeoff begins to exceed that for shakeup approximately 50 eV above threshold. The probability for $3p$ shakeoff rises very slowly; in the sudden-approximation limit, it is expected to exceed the shakeup probability by a factor of 8.8.

The observed onset of $1s3p$ absorption at 14 559±2 eV and the rise of the total two-electron absorption to 38±5 b at 14 587 eV agree within uncertainties with a previous observation [46]. The clear spin-orbit splitting of the $[1s3p]$ double-hole state, observed by Deutsch and Hart [46], is not apparent in the present data.

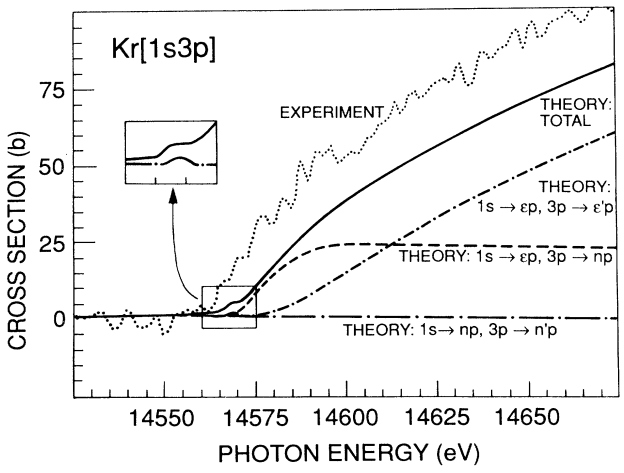

FIG. 5. Experimental Kr $1s3p$ double-photoexcitation cross section (dotted curve), compared with calculated partial cross sections: double bound-bound transitions (dots and long dashes), $3p$ shakeup transitions (dashed curve), $3p$ shakeoff transitions (dash-dotted curve), and the sum of theoretical partial cross sections (solid curve). For clarity, the theoretical double bound-bound and total cross sections in the 1460–1475-eV photon-energy range are shown enlarged in the inset.

4. *Kr* [*1s2s*] *and* [*1s2s4p*]

An attempt to observe the $1s2s$ absorption threshold must be guided by accurate energy and cross-section calculations because of the very small magnitude of the expected feature. The calculated theoretical Kr $1s2s$ absorption cross section exhibits only a change in slope at threshold of 5.6×10^{-3} b/eV. Detection of such a small change in slope is exceedingly difficult because the calculated underlying cross-section components have a magnitude of ~14 100 b, with a slope of −2.3 b/eV near 16 400 eV.

The measured and calculated absorption cross sections in the Kr $1s2s$ two-electron excitation region are shown in Fig. 6; the pertinent energy calculations are discussed in Sec. II C 2. Triple $1s2s4p$ excitations, with a threshold 15 eV above the $1s2s$ thresholds, are calculated to occur with a substantial relative probability of 0.5±0.2 of the double excitations.

The measured absorption cross section of ~13 500 b exhibits an apparent jump of ~2 b at a photon energy ~30 eV above the calculated $[1s2s]\,^3S$ threshold (Fig. 6). This feature appears in independent combinations of data

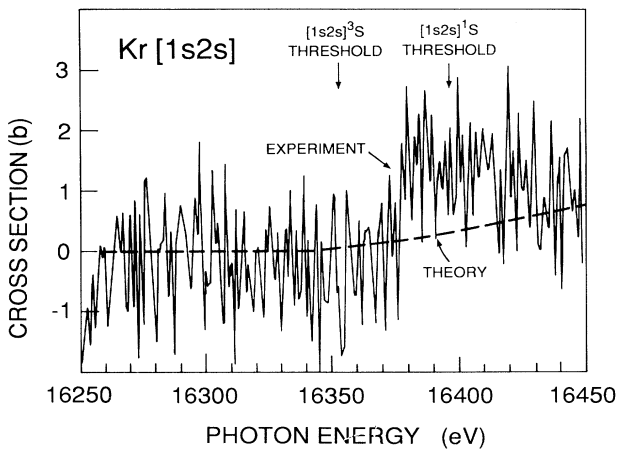

FIG. 6. Measured Kr photoabsorption cross section in the $1s2s$ threshold region, with background subtracted as described in the text (solid curve), compared with the theoretical cross section for transitions to $[1s2s\,^3S]$, $[1s2s\,^1S]$, and $[1s2s\,^3S4p]$ final states. The step in the data near 16 380 eV is believed to be spurious.

sets from which "bad" spectra (judged by a χ^2 criterion) were eliminated. If ascribed to a real change in Kr photoabsorption, the step would correspond to a decrease of ~ 10 counts in I_1 out of $\sim 3.4\times 10^5$ counts. Data sets evaluated with the function $\ln(\sum_n I_0/\sum_n I_1)$ and with $\ln[(1/n)\sum_n (I_0/I_1)]$ differ by $<10\%$ in standard deviation. A fit of a simple step function to $\ln(\sum I_0/\sum I_1)$ for one data set exhibits a 1.29σ step at (16 377.0±4.8)-eV photon energy; a fit to an independent data set indicates a 1.48σ step at 16 380.0±4.0 eV, the uncertainty in energies being the result of the ±1.3-eV uncertainty in the calibration throughout the experiments and of the statistical uncertainties in the data. In a background measurement with an air-filled target chamber, a similar fit indicates a 1.25σ step at 16 385±5.0 eV. Furthermore, the edge in Fig. 6 corresponds neither in shape, nor in energy, nor in magnitude to the predictions from *ab initio* theory (Sec. II B 2 and II C 2). We therefore conclude that the feature most likely is spurious and should be ascribed to an artifact, such as a change of unknown origin in harmonic content of the x-ray beam—it is readily calculated that a change in lowest-harmonic intensity from 1.00% to 0.97% of the fundamental would cause an apparent $\sim$2-b increase in the cross section. The observation illustrates how readily spurious absorption features at this level can mimic multielectron-excitation signals. The reported edge [46] of 10.1±2.6 b at 16 279 eV was not observed in this experiment.

V. SUMMARY AND CONCLUSIONS

The probability of Kr $1s$ ionization alone and accompanied by excitation of a $4p$, $3d$, $3p$, $2s$, or a $2s$ and $4p$ electron into bound or continuum states has been calculated for a photon-energy range extending a few hundred eV above the respective thresholds. The $1s$ ionization cross section was calculated relativistically including complete relaxation. Two-electron photoexcitation and ionization was calculated with Hatree-Fock wave functions, except for transitions to $[1sns]$ final states, for which Dirac-Fock wave functions were employed. The multiple photoexcitation computations were carried out within the dipole approximation; configuration interaction in the final state and conjugate shake processes were neglected. Pertinent energy thresholds were calculated relativistically, including dynamic correlation effects, Breit energy, and quantum electrodynamic corrections.

The calculations show that sharp features from two-electron excitations are produced in an absorption spectrum only if at least one electron undergoes a bound-bound transition; if both electrons are promoted into the continuum, the total absorption cross section exhibits only a slight change in slope. For more tightly bound electrons, shakeoff tends to prevail increasingly over shakeup, whence double-excitation features from inner-shell electrons become elusive.

An absorption-spectrometry measurement was carried out with synchrotron radiation in order to test the calculations. Near the K edge of Kr, the measured absorption substantially exceeds the theoretical curve, even after bound-bound excitations are included in the calculated $1s$ single-electron photoabsorption cross section. For double-electron excitations, a background-subtraction technique employed here permitted analysis of the $1s3d$ and $1s3p$ cross sections as far as $\sim$130 eV above threshold. The observed slow rise in double-electron absorption due to shakeoff processes in $1s3d$ and $1s3p$ transitions agrees rather well with theory. The more tightly the electrons are bound, the more slowly the double-electron cross sections are found to rise with photon energy, in accord with theory.

Threshold cross sections for $1s4p$, $1s3d$, and $1s3p$ transitions are poorly predicted by the single-configuration Hartree-Fock calculations, most likely because the model does not include initial- and final-state configuration interaction nor contributions from conjugate shake and direct collisions. The $1s4p$ cross section was difficult to derive from the data because of the proximity of the K edge, yet it is clear that the theory greatly overestimates $4p$ shakeup near threshold.

For $1s2s$ photoexcitation, only a very slight change in slope of the total absorption cross section is predicted at threshold, which would make it difficult to measure with present-day facilities. Triply excited $[1s2s4p]$ states are calculated to occur with high probability, approximately half that of producing $[1s2s]$ double-hole states. The data exhibit an apparent edge in the $1s2s$ excitation region which, however, agrees with theory neither in energy nor in magnitude and is most likely due to extraneous effects. With improvements in techniques and in synchrotron-radiation sources, it may become possible in future to measure these extreme inner-shell multielectron photoexcitation processes, including the splitting of $[1sns]$ double-hole states predicted to arise from the spin dependence of the relativistic Breit-Coulomb Hamiltonian.

ACKNOWLEDGMENTS

We are indebted to Pierre Capeder and Chuck Troxel, Jr. for valuable technical assistance during the experiment; we wish to thank Britt Hedman for her generous advice on software and Honghong Wang for her help with data processing. One of us (A.F.K.) acknowledges support from the Fulbright Foundation, administered through the Council for International Exchange of Scholars. In the University of Oregon, this work was supported in part by the National Science Foundation and in the Helsinki University of Technology, by the Academy of Finland. In the Lawrence Livermore National Laboratory, the research was performed under the auspices of the U.S. Department of Energy under Contract No. W-7405-ENG-48. In the Argonne National Laboratory, this research was supported by the U.S. Department of Energy, Division of Chemical Sciences, Office of Basic Energy Sciences, under Contract No. W-31-109-ENG-38. The experiment was carried out at SSRL, which is operated by the Department of Energy, Division of Chemical Sciences.

*Present address: Department of Physics, University of Central Florida, Orlando, FL 32816.
†Permanent address: J. Stefan Institute, University of Ljubljana, 61111 Ljubljana, Slovenia.

[1] M. O. Krause, T. A. Carlson, and R. D. Dismukes, Phys. Rev. **170**, 37 (1968).
[2] T. Åberg, Phys. Rev. **156**, 35 (1967).
[3] T. Åberg, Ann. Acad. Sci. Fenn. A VI **308**, 1 (1969).
[4] T. Åberg, in *Proceedings of the International Conference on Inner-Shell Ionization Phenomena and Future Applications,* edited by R. W. Fink, S. T. Manson, J. M. Palms, and P. Venugopala Rao, U. S. AEC Report No. CONF-720404 (National Technical Information Service, U.S. Department of Commerce, Springfield, VA, 1972), p. 1509.
[5] U. Gelius, J. Electron Spectrosc. **5**, 985 (1974).
[6] R. L. Martin and D. A. Shirley, in *Electron Spectroscopy,* edited by C. R. Brundle and D. A. Baker (Academic, New York, 1977), Vol. 1, Chap. 2.
[7] J. Tulkki, Phys. Rev. Lett. **62**, 2817 (1989).
[8] L. Asplund, P. Kelfve, B. Blomster, H. Siegbahn, and K. Siegbahn, Phys. Scr. **16**, 268 (1977).
[9] G. B. Armen, T. Åberg, K. R. Karim, J. C. Levin, B. Crasemann, G. S. Brown, M. H. Chen, and G. E. Ice, Phys. Rev. Lett. **54**, 182 (1985).
[10] R. D. Deslattes, R. E. LaVilla, P. L. Cowan, and A. Henins, Phys. Rev. A **27**, 923 (1983).
[11] A. Kodre, S. J. Schaphorst, and B. Crasemann, in *X-Ray and Inner-Shell Processes,* edited by T. A. Carlson, M. O. Krause, and S. T. Manson, AIP Conf. Proc. No. 215 (AIP, New York, 1990), p. 582, and references therein.
[12] B. Crasemann, Comments At. Mol. Phys. **22**, 163 (1989).
[13] A. Fahlman, M. O. Krause, T. A. Carlson, and A. Svensson, Phys. Rev. A **30**, 812 (1984).
[14] U. Becker, B. Langer, H. G. Kerkhoff, M. Kupsch, D. Szostak, R. Wehlitz, P. A. Heiman, S. H. Liu, D. W. Lindle, T. A. Ferrett, and D. A. Shirley, Phys. Rev. Lett. **60**, 1490 (1988).
[15] M. O. Krause and C. D. Caldwell, Phys. Rev. Lett. **59**, 2736 (1987).
[16] B. Crasemann, J. Phys. (Paris) **48**, C9-389 (1987).
[17] G. Wentzel, Ann. Phys. (Leipzig) **66**, 437 (1921).
[18] W. Heisenberg, Z. Phys. **32**, 841 (1925).
[19] M. J. Druyvesteyn, Z. Phys. **43**, 707 (1927).
[20] F. K. Richtmyer, J. Frank. Inst. **208**, 325 (1929).
[21] F. Bloch, Phys. Rev. **48**, 187 (1935).
[22] W. Wölfli, Ch. Stoller, G. Bonani, M. Suter, and M. Stockli, Phys. Rev. Lett. **35**, 656 (1975).
[23] A. E. Sandström, in *X-Rays,* edited by S. Flügge, Handbuch der Physik Vol. XXX (Springer-Verlag, Berlin, 1957), Sec. I.6, p. 78.
[24] T. A. Carlson, Phys. Rev. **130**, 2361 (1963).
[25] T. A. Carlson and M. O. Krause, Phys. Rev. **137**, A1655 (1965).
[26] T. A. Carlson and M. O. Krause, Phys. Rev. **140**, A1057 (1965).
[27] H. W. Schnopper, Phys. Rev. **131**, 2558 (1963).
[28] R. P. Madden and K. Codling, Phys. Rev. Lett. **10**, 516 (1963).
[29] J. W. Cooper, U. Fano, and F. Prats, Phys. Rev. Lett. **10**, 518 (1963).
[30] We follow the convention of designating vacancies by square brackets.
[31] A. Kodre, M. Hribar, I. Arčon, D. Glavič-Cindro, M. Štuhec, R. Frahm, and W. Drube, Phys. Rev. A **45**, 4682 (1992).
[32] S. I. Salem, Brahm Dev, and P. L. Lee, Phys. Rev. A **22**, 2679 (1980).
[33] S. I. Salem, D. D. Little, A. Kumar, and P. L. Lee, Phys. Rev. A **24**, 1935 (1981).
[34] S. I. Salem, A. Kumar, and P. L. Lee, Phys. Lett. **92A**, 331 (1982).
[35] M. Deutsch and M. Hart, Phys. Rev. A **29**, 2946 (1984).
[36] M. Deutsch, M. Hart, and P. Durham, J. Phys. B **17**, L395 (1984).
[37] S. I. Salem, A. Kumar, and P. L. Lee, Phys. Rev. A **25**, 2069 (1982).
[38] S. I. Salem, A. Kumar, K. G. Schiessel, and P. L. Lee, Phys. Rev. A **26**, 3334 (1982).
[39] A. Kumar, B. L. Scott, and S. I. Salem, J. Phys. B **18**, 3105 (1985).
[40] S. I. Salem and A. Kumar, J. Phys. B **9**, 73 (1986).
[41] G. Li, F. Bridges, and G. S. Brown, Phys. Rev. Lett. **68**, 1609 (1992).
[42] See, for example, L. V. Azároff, R. Kaplow, N. Kato, R. J. Weiss, A. J. C. Wilson, and R. A. Young, *X-Ray Diffraction* (McGraw-Hill, New York, 1974), p. 547.
[43] J. M. Esteva, B. Gauthé, P. Dhez, and R. C. Karnatak, J. Phys. B **16**, L263 (1983).
[44] S. Bodeur, P. Millie, E. Lizon a Lugrin, I. Nenner, A. Filipponi, F. Boscherini, and S. Mobilio, Phys. Rev. A **39**, 5075 (1989).
[45] U. Kuetgens and J. Hormes, Phys. Rev. A **44**, 264 (1991).
[46] M. Deutsch and M. Hart, Phys. Rev. Lett. **57**, 1566 (1986).
[47] M. Deutsch and M. Hart, Phys. Rev. A **34**, 5168 (1986).
[48] R. Frahm, W. Drube, I. Arčon, D. Glavič-Cindro, M. Hribar, and A. Kodre (unpublished), as quoted in [11], and Ref. [31].
[49] E. Bernieri and E. Burattini, Phys. Rev. A **35**, 3322 (1987).
[50] Y. Ito, H. Nakamatsu, T. Mukoyama, K. Omote, S. Yoshikado, M. Takahashi, and S. Emura, Phys. Rev. A **46**, 6083 (1992).
[51] M. Deutsch and P. Kizler, Phys. Rev. A **45**, 2112 (1992).
[52] C. Dezarnaud, F. Guillet, and M. Tronc, J. Phys. B **25**, L123 (1992).
[53] V. L. Sukhorukov, A. N. Hopersky, I. D. Petrov, V. A. Yavna, and V. F. Demekhin, J. Phys. (Paris) **48**, 1677 (1987).
[54] "Third-generation" synchrotron-radiation facilities are designed to derive radiation primarily from undulators. The first of these machines to come on line in the United States will be the Advanced Light Source in the Lawrence Berkeley Laboratory and the Advanced Photon Source in the Argonne National Laboratory.
[55] J. H. Scofield, Lawrence Livermore Radiation Laboratory Report No. UCRL-51326, 1973 (unpublished).
[56] C. S. Fadley, Chem. Phys. Lett. **25**, 225 (1974); T. Åberg, in *Photoionization and Other Probes of Many-Electron Interactions,* edited by F. J. Wuilleumier (Plenum, New York, 1976), p. 49.
[57] J. H. Hubbell and W. J. Veigele, *Comparison of Theoretical and Experimental Photoeffect Data 0.1 keV to 1.5 MeV,* Natl. Bur. Stand. (U.S.) Technical Note No. 901 (U.S. GPO, Washington, DC, 1976).
[58] E. B. Saloman, J. H. Hubbell, and J. H. Scofield, At. Data Nucl. Data Tables **38**, 1 (1988); E. B. Saloman and J. H. Hubbell, *X-Ray Attenuation Coefficients (Total Cross Sections): Comparison of the Experimental Data Base with the Recommended Values of Henke and the Theoretical Values*

of Scofield for Energies Between 0.1–100 keV, Natl. Bur. Stand. (U.S.) Technical Note No. NBSIR 86-3431 (U.S. GPO, Washington, DC, 1986).
[59] W. Jitschin, U. Werner, G. Materlik, and G. D. Doolen, Phys. Rev. A **35**, 5038 (1987).
[60] J. Tulkki and T. Åberg, J. Phys. B **18**, L489 (1985).
[61] M. Ya. Amusia, V. K. Ivanov, and V. A. Kupchenko, J. Phys. B **14**, L667 (1981).
[62] J. Tulkki, G. B. Armen, T. Åberg, B. Crasemann, and M. H. Chen, Z. Phys. D **5**, 241 (1987).
[63] G. B. Armen, J. Tulkki, T. Åberg, and B. Crasemann, Phys. Rev. A **36**, 5606 (1987).
[64] T. Åberg, Phys. Scr. **21**, 495 (1980).
[65] T. Åberg, in *Inner-Shell and X-Ray Physics of Atoms and Solids,* edited by D. J. Fabian, H. Kleinpoppen, and L. M. Watson (Plenum, New York, 1981), p. 251.
[66] T. Åberg and J. Tulkki, in *Atomic Inner-Shell Physics,* edited by B. Crasemann (Plenum, New York, 1985), p. 419.
[67] A. F. Starace, in *Corpuscles and Radiation in Matter I,* edited by S. Flügge and W. Mehlhorn, Handbuch der Physik Vol. XXI (Springer, Berlin, 1982), p. 1.
[68] I. P. Grant, B. J. McKenzie, P. H. Norrington, D. F. Mayers, and N. C. Pyper, Comput. Phys. Commun. **21**, 207 (1980).
[69] J. Tulkki, Phys. Rev. A **32**, 3153 (1985).
[70] J. Tulkki, T. Åberg, A. Mänttykenttä, and H. Aksela, Phys. Rev. A **46**, 1357 (1992).
[71] W. Mehlhorn, in *Atomic Inner-Shell Physics* (Ref. [66]), Chap. 4.
[72] T. Åberg and G. Howat, in *Corpuscles and Radiation in Matter I* (Ref. [67]), p. 469; T. Åberg, Phys. Scr. **T41**, 71 (1992).
[73] T. N. Chang, T. Ishihara, and R. T. Poe, Phys. Rev. Lett. **27**, 838 (1971).
[74] T. A. Ferrett, D. W. Lindle, P. A. Heimann, W. D. Brewer, U. Becker, H. G. Kerkhoff, and D. A. Shirley, Phys. Rev. A **36**, 3172 (1987).
[75] S. T. Manson, Adv. Electron. Electron Physics **41**, 73 (1976).
[76] D. L. Wark, R. Bartlett, T. J. Bowles, R. G. H. Robertson, D. S. Sivia, W. Trela, J. F. Wilkerson, G. S. Brown, B. Crasemann, S. L. Sorensen, S. J. Schaphorst, D. A. Knapp, J. Henderson, J. Tulkki, and T. Åberg, Phys. Rev. Lett. **67**, 2291 (1991).
[77] R. L. Martin and D. A. Shirley, Phys. Rev. A **13**, 1475 (1976).
[78] C. Froese Fischer, Comput. Phys. Commun. **14**, 145 (1978).
[79] G. B. Armen, Ph.D. thesis, University of Oregon, 1985.
[80] P. O. Löwdin, Phys. Rev. **97**, 1474 (1953).
[81] G. B. Armen, B. I. Craig, F. P. Larkins, and J. A. Richards, J. Electron Spectrosc. Relat. Phenom. **51**, 183 (1990).
[82] R. D. Cowan, *The Theory of Atomic Structure and Spectra* (University of California Press, Berkeley, 1981).
[83] For a review of theoretical atomic binding-energy calculations, see, e.g., B. Crasemann, Kh. R. Karim, and M. H. Chen, At. Data Nucl. Data Tables **36**, 355 (1987).
[84] D. A. Liberman, D. T. Cromer, and J. T. Waber, Comput. Phys. Commun. **2**, 107 (1971).
[85] A. Rosén and I. Lindgren, Phys. Rev. **176**, 114 (1968).
[86] K.-N. Huang, M. Aoyagi, M. H. Chen, B. Crasemann, and H. Mark, At. Data Nucl. Data Tables **18**, 243 (1976).
[87] M. H. Chen, B. Crasemann, M. Aoyagi, K.-N. Huang, and H. Mark, At. Data Nucl. Data Tables **26**, 561 (1981).
[88] J. B. Mann and W. R. Johnson, Phys. Rev. A **4**, 41 (1971).
[89] M. H. Chen, B. Crasemann, N. Mårtensson, and B. Johansson, Phys. Rev. A **31**, 556 (1985).
[90] P. J. Mohr, Ann. Phys. (N.Y.) **88**, 52 (1974); Phys. Rev. Lett. **34**, 1050 (1975); Phys. Rev. A **26**, 2338 (1982).
[91] K.-N. Huang, Phys. Rev. A **14**, 1311 (1976).
[92] M. H. Chen, Phys. Rev. A **31**, 1449 (1985).
[93] I. P. Grant, in *X-Ray and Inner-Shell Processes* (Ref. [11]), p. 46.
[94] B. T. Pickup and O. Goscinski, Mol. Phys. **26**, 1019 (1973).
[95] M. Ohno and G. Wendin, J. Phys. B **11**, 1557 (1979); **12**, 1305 (1979).
[96] M. H. Chen, B. Crasemann, and H. Mark, Phys. Rev. A **24**, 1158 (1981).
[97] Kh. R. Karim and B. Crasemann, Phys. Rev. A **31**, 709 (1985).
[98] M. H. Chen, B. Crasemann, and H. Mark, Phys. Rev. A **25**, 391 (1982).
[99] A. E. Sandström, Z. Phys. **65**, 632 (1930).
[100] T. Matsushita and H.-O. Hashizume, in *Handbook on Synchrotron Radiation,* edited by E.-E. Koch (North-Holland, Amsterdam, 1983), Vol. 1a, p. 261.
[101] M. Breinig, M. H. Chen, G. E. Ice, F. Parente, B. Crasemann, and G. S. Brown, Phys. Rev. A **22**, 520 (1980).
[102] K. Siegbahn, C. Nordling, G. Johansson, J. Hedman, P. F. Hedén, K. Hamrin, U. Gelius, T. Bergmark, L. O. Werme, R. Manne, and Y. Baer, *ESCA Applied to Free Molecules* (North-Holland, Amsterdam, 1969).
[103] K. G. Dyall, J. Phys. B **16**, 3137 (1983).
[104] M. Deutsch and M. Hart, J. Phys. B **19**, L303 (1986).
[105] M. O. Krause and J. H. Oliver, J. Phys. Chem. Ref. Data **8**, 329 (1979).
[106] M. Deutsch, G. Brill, and P. Kizler, Phys. Rev. A **43**, 2591 (1991).
[107] O. Keski-Rahkonen, Phys. Scr. **7**, 173 (1973).
[108] J. W. Cooper, Phys. Rev. A **38**, 3417 (1988).